

See discussions, stats, and author profiles for this publication at: <https://www.researchgate.net/publication/376471192>

A DATA-SPARSE APPROACH TO IN-SITU FAULT DETECTION AND IDENTIFICATION FOR METAL ADDITIVE MANUFACTURING

Conference Paper · September 2023

DOI: 10.12783/shm2023/36939

CITATIONS

0

READS

24

3 authors, including:



Alvin Chen

Rensselaer Polytechnic Institute

5 PUBLICATIONS 5 CITATIONS

SEE PROFILE



Fotis Kopsaftopoulos

Rensselaer Polytechnic Institute

125 PUBLICATIONS 1,837 CITATIONS

SEE PROFILE

A Data-sparse Approach to In-situ Fault Detection and Identification for Metal Additive Manufacturing

ALVIN CHEN, FOTIS KOPSAFTOPOULOS
and SANDIPAN MISHRA

ABSTRACT

With increasing adoption of metal additive manufacturing (AM) in manufacturing, detecting faults in the printing process has the potential to reduce waste from failed prints and streamline the production process. To increase robustness of anomaly detection, a statistical method of detecting faults from melt pool images is presented. This method uses parametric identification of 1D compression of melt pool images to build a nominal predictive model. Nominal melt pools result in residuals that are Gaussian white noise processes, whereas anomalous melt pools will not follow this distribution. Detection is performed through statistical comparison of incoming data with a nominal reference generated on sparse data. This approach successfully applies statistical time-series methods to detect anomalous melt pools in a metal AM process.

INTRODUCTION

Identifying faults in a metal additive manufacturing (AM) process is a critical step in increasing adoption of the technology. Metal AM processes are prone to faults, frequently stopping the print, or resulting in products with inadequate physical properties [1]. Among the methods that are used to monitor the process, one common technique is through the imaging of the melt pool formed by the laser sintering powder material together [2]. This melt pool image reflects the dynamics of the system, as its shape and size correspond to the quality of the sinter [3]. Furthermore, several faults directly appear within these images, motivating its use for in-situ fault detection.

Most detection approaches focus on image classification, matching melt pool images with known datasets of anomalous signals [4]. These methods use neural network (NN)

Alvin Chen, PhD Student, Email: chena17@rpi.edu, Intelligent Structural Systems Lab (ISSL), Department of Mechanical, Aerospace and Nuclear Engineering, Rensselaer Polytechnic Institute, Troy, NY, USA.

Fotis Kopsaftopoulos, Assistant Professor. Intelligent Structural Systems Lab (ISSL), Department of Mechanical, Aerospace and Nuclear Engineering, Rensselaer Polytechnic Institute, Troy, NY, USA.

Sandipan Mishra, Professor. Intelligent Systems, Automation and Control (ISAaC), Department of Mechanical, Aerospace and Nuclear Engineering, Rensselaer Polytechnic Institute, Troy, NY, USA.

models, which require large, labelled datasets. The data collection process is slow for AM and may not account for all potential faults. Furthermore, these methods do not incorporate the effects of geometry into the detection process by inspecting images independently. The raster chosen for the cross-sectional layers affects the melt pool signal and microstructure of the print, altering the melt pool image sequence without inducing fault [5,6]. To detect these geometry-based effects, time series methods can be used, such as in [7], where time series data was used to detect voids in metal AM printed parts. However, this approach uses a NN and requires a large, labelled dataset.

Incorporating the effects of geometry into detection capabilities is possible by examining the time series, as explained in prior work [8,9]. The melt pool image time series comprises pertinent print geometry information, however few methods explore this signal for fault detection [10]. Furthermore, to reduce reliance on labeled datasets, a detection methodology that statistically determines the closeness of sample data to a nominal baseline can be used. Statistical time series approaches can increase the detection capabilities by incorporating geometric properties into the nominal model while lessening the data requirement [11].

The goal of this work is to establish a statistical method of detecting faults in a metal AM process by modeling a time series of compressed 1D melt pool images. For a laser powder bed fusion (LPBF) process, the major axis of a fit ellipse on the melt pool is used to reduce image dimensionality. The major axis corresponds to melt pool size along the print direction, defining the shape simply while reducing effects from varying scan paths. Other compression metrics can be used (as in prior work [8,9]), although anomalies that alter melt pool shape distinctly appear in the chosen time series. An AutoRegressive (AR) model predicts the time series, modelling the geometric properties of the raster. To perform detection, the residuals derived from the model error are used. These residuals will naturally be Gaussian, as the melt pool size is typically Gaussian, with fluctuations from the periodic raster.

Using these residuals, we can use well-defined statistical methods [12] to determine how well the residuals of any print layer conform to the expected nominal behavior. Faults will result in dissimilar residuals, as the nominal AR model will not be able to remove the anomalous response from the residuals. Furthermore, the reference nominal parameters can be determined from only one layer, reducing the quantity of data necessary for detection.

The main contributions of this study are:

1. An application of an AR model to predict the compressed melt pool time series from sparse data (one test layer per raster pattern).
2. The implementation of a statistical detection methodology for metal AM using a time series model. The detection method is based on the expected normal distribution of the model residuals and does not require labels to detect anomalies.

EXPERIMENTAL SETUP

Melt pool images are obtained in-situ by means of a coaxial near infrared (NIR) camera. This camera obtains 64×64 pixel greyscale images at a rate of 2 kHz. The

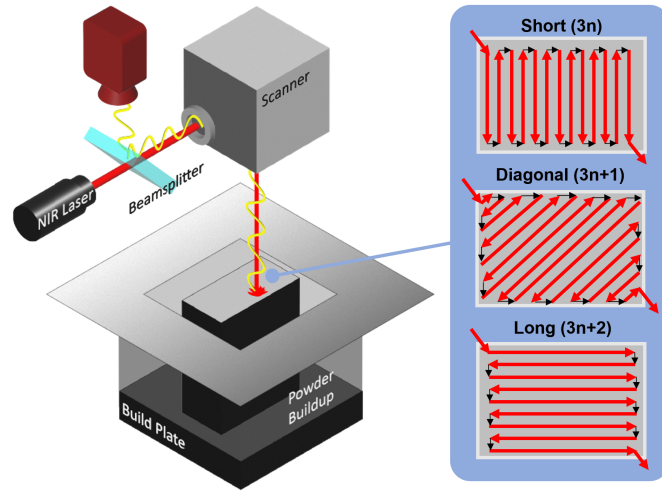


Figure 1. Sensor configuration (left) and chosen raster patterns (right). A coaxial camera monitors the melt pool during the printing process. Three raster patterns are chosen to construct a $2 \times 4\text{cm}$ rectangular prism. The raster patterns are composed of lines alternating directions, resulting in "turnaround" locations along the edges. These locations have high energy deposition, inducing periodic increases in the melt pool size dependent on the raster interval.

camera arrangement is depicted in Figure 1 and is identical to prior work [8, 9]. The coaxial camera is able to record the melt pools along this path through the reflection of the melt pool through the scanner, capturing the melt pool image regardless of scanner position.

The dataset consists of 50 layers printed of a $2 \times 4\text{cm}$ rectangular prism. The scanner follows 3 raster paths to sinter cross-sectional layers, illustrated in figure 1: 90° , 45° , and 0° degrees, corresponding to the short, diagonal, and long directions, respectively.

The melt pool size is quantified by taking the major axis of the ellipse formed by the melt pool image, as shown in figure 2. The ellipse is estimated for the silhouette of the image with pixel values above a threshold. For this work, the threshold was chosen to be pixels with values of at least 50 out of the maximum 255, although other thresholds can be chosen. This melt pool length measurement forms the $1D$ signal used for modeling and detection.

Fluctuations in the melt pool length arise from the geometric periodicity. At locations of dense raster patterns (such as at spots where the laser path turns back on itself), the local energy density will increase, consequently increasing the melt pool size. This geometric effect is deterministic, depending on the chosen raster pattern and can thus be modeled. For nominal images, as illustrated in figure 2, the major axis will follow the geometric periodicity, with few deviations from the expected size. In contrast, anomalous melt pools will experience greater variance, and the model will not be able to capture this behavior well.

The time series data was filtered through a low pass filter (cutoff frequency 255Hz) to remove high frequencies, as geometry-based system dynamics occur at frequencies below this threshold. The dataset was down sampled to 1kHz to reduce AR model order. Each layer takes approximately 5.5 seconds to print, yielding about 5500 samples per layer (after down sampling).

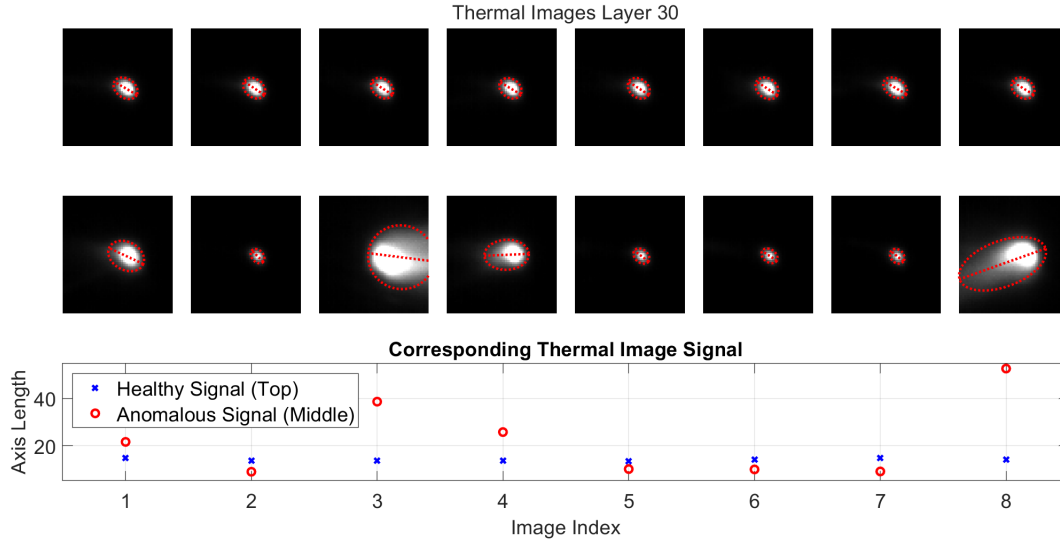


Figure 2. Sample melt pool images with ellipse shape approximation. The major axis of the ellipse approximation is marked across the melt pool in red. Healthy (Top) and unhealthy (middle) melt pools exhibit different sizes. The major axis length (bottom) follows a normal distribution, with anomalous signals varying from nominal.

TIME SERIES MODELING AND STATISTICAL DECISION MAKING

A statistical hypothesis test is implemented to detect faults by comparing the distribution of AutoRegressive (AR) model residuals to that of known nominal data. Under the null hypothesis, the AR model will capture the effects of geometry, and the residuals will be independent and identically distributed (iid) random variables with nominal variance σ_{oo}^2 . In the event of an anomaly, the null hypothesis will not hold and the residual distribution will exceed the nominal, declaring a fault. This method has been implemented successfully in other applications [12].

The linear time invariant AR model is used for its simplicity, however time-varying models can be used for raster patterns that induce time-varying behavior in the time series. Investigation of these other modeling techniques is the subject of future work.

AR Model

The AR model of order na is of the following form [13]:

$$y[t] + \sum_{i=1}^{na} a_i \cdot y[t-i] = e[t] \quad e[t] \sim \text{iid}\mathcal{N}(0, \sigma_e^2) \quad (1)$$

with normalized discrete time $t = 1, \dots, N$. Absolute time is $t_a = T_s(t-1)$ with sampling time T_s . $e[t]$ is the 1-step model residual sequence that is expected to be an independent and identically distributed (iid), white, Gaussian, zero mean sequence with variance σ_e^2 . This is indicated by the symbol $\mathcal{N}(\cdot, \cdot)$ with the respective mean and variance. Parameters a_1, a_2, \dots, a_{na} are estimated by minimization of a least squares fit [13]. Model selection is achieved by selecting a model order na with minimal Bayesian information criterion (BIC) when fitting AR models of increasing order to nominal layers.

For nominal data, the residuals are expected to be iid normally distributed with a mean of zero. The variance of the residuals are estimated for N samples as:

$$\hat{\sigma}_e^2 = \frac{1}{N} \sum_{i=1}^N e[i]^2 \quad (2)$$

Statistical Hypothesis Test

Detection is based on the following binary hypothesis test:

$$\begin{aligned} H_0 : \sigma_{oo}^2 &= \sigma_{ou}^2 && \text{Null Hypothesis - Healthy Signal} \\ H_1 : \sigma_{oo}^2 &< \sigma_{ou}^2 && \text{Alternative Hypothesis - Anomalous Signal} \end{aligned} \quad (3)$$

For nominal layers, the AR model is accurate, and the variance of the residuals $e_{oo}[t]$ achieve a minimum value, σ_{oo}^2 . Sample signals, when driven through the AR model, result in residuals $e_{ou}[t]$ with variance σ_{ou}^2 . Under the null hypothesis, these residuals $e_{ou}[t]$ will be like the nominal residuals $e_{oo}[t]$, iid zero mean Gaussian with variance σ_{oo}^2 . Anomalous signals, when driven through the AR model, will yield residuals with variance above the nominal.

We form a test statistic to formalize detection using the variance estimation for test variance $\hat{\sigma}_{ou}^2$ and nominal variance $\hat{\sigma}_{oo}^2$. Nominal variance $\hat{\sigma}_{oo}^2$ is estimated using Equation 2 from one set of nominal layer residuals $e_o[t], t = na, \dots, N_o$. Sample variances $\hat{\sigma}_{ou}^2$ are estimated from a moving window M with $M - 1$ overlapping samples across the layer residuals $e_{ou}[t], t = na, \dots, N_u$. This becomes a variance vector of length $N_u - (M - na) + 1$ across the layer corresponding to times $t = M + na, \dots, N_u$. The variances each follow a central χ^2 distribution (as a sum of iid normal random variables), and thus the ratio follows a f distribution with degrees of freedom $(M, N_o - na)$ for model order na . M, N_o correspond to the number of samples used to estimate σ_{ou}^2 and σ_{oo}^2 , respectively. The statistical threshold for a type I risk level (α) is then:

$$\begin{aligned} F &= \frac{\hat{\sigma}_{ou}^2}{\hat{\sigma}_{oo}^2} \sim f(M, N_o - na) \\ F &\leq f_{1-\alpha}(M, N_o - na) && H_0 \text{ accepted - Nominal Signal} \\ \text{Else} &&& H_1 \text{ accepted - Anomalous Signal} \end{aligned} \quad (4)$$

FAULT DETECTION PERFORMANCE

One AR model for each raster pattern was selected as the nominal model. To choose the best model order, the order with minimum Bayesian information criteria (BIC) was selected. The chosen model orders for each raster pattern are illustrated in figure 3. The orders chosen are 95, 106, and 106 for the short, diagonal, and long directions, respectively. Each AR was fit using one nominal layer (5500 samples).

The residuals for six sample layers (two per raster direction) are presented in Figure 4. In all raster directions, the nominal layers (top rows) remain consistent to the expected mean of 0, whereas anomalous layers (bottom rows) exhibit peaks and wider variances

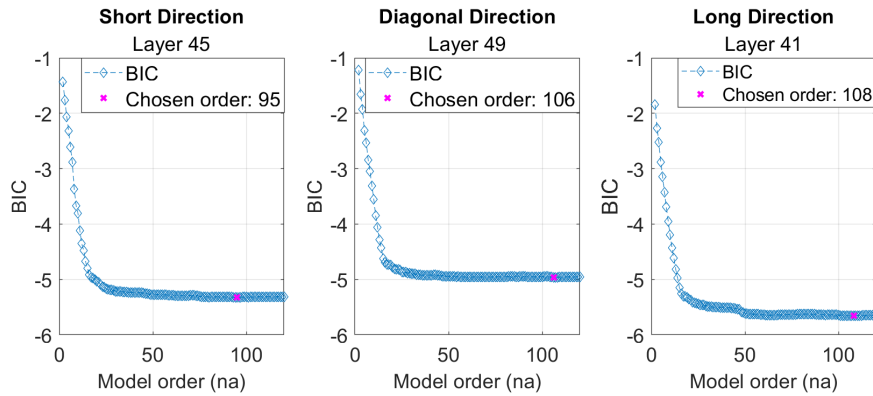


Figure 3. BIC curves and chosen model order (magenta x) for each raster pattern (Short, Diagonal, and Long, from left to right). Model orders of 95, 106, and 108 were chosen for the listed raster patterns, respectively. One model was used for each raster pattern to best capture the geometry-based effects.

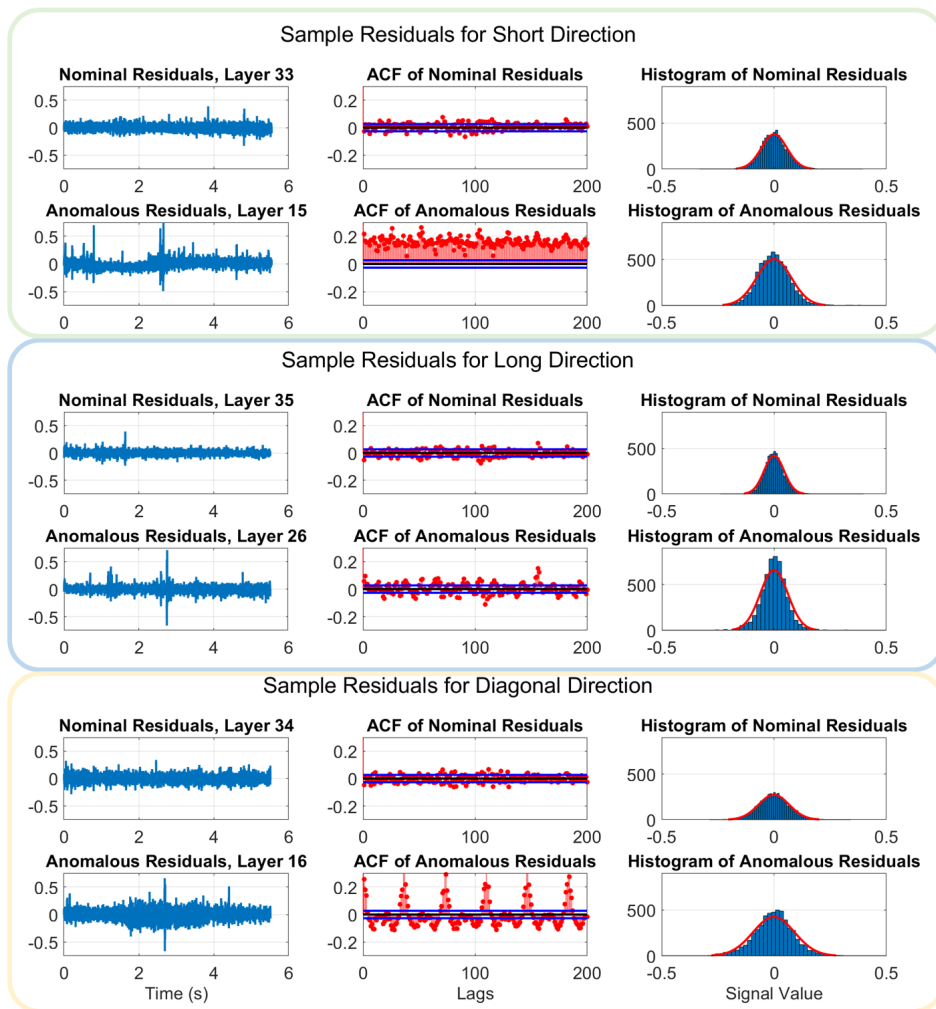


Figure 4. Nominal (top row) and anomalous (bottom row) residuals of sample layers for each raster direction. Model residuals (left) are white for nominal data. The ACF (center) visualizes the whiteness of the residuals. The histogram (right) shows the distribution of the data. Anomalous data has a distinct distribution compared to nominal.

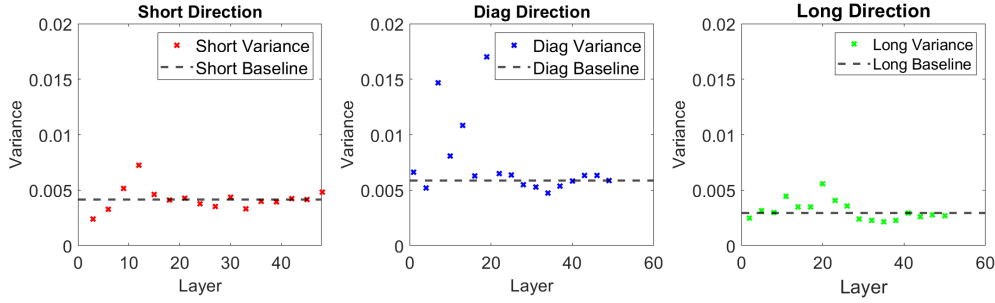


Figure 5. Baseline variances of model residuals generated by filtering layer signals through the baseline AR model (separated by raster direction). The healthy reference was chosen to be approximately the mean of nominal variances.

at fault locations. Accordingly, the nominal layers have white residuals, as no anomalies occur within these layers. The nominal model is predicting the geometric effects of the raster, removing the periodicity and leaving the residuals white. In contrast, the anomalous layers have residuals with a clear periodicity (non-zero autocorrelation function). This implies that irregular melt pool sizes occur within this layer, which is indicative of an anomaly. This can be seen in the corresponding histogram where anomalous layers have a distinct distribution compared to the nominal layer.

We quantify the deviation of the residuals by the variance. For nominal models, the residuals will have a lower variance as seen in the previous figures. As anomalous signals have non-white residuals, the variance will be higher for layers with anomalies. We can then use equation 3 and 4 to formalize this detection criteria. We choose a reference nominal variance σ_{oo}^2 by first inspecting the variance of nominal models. This can be seen in Figure 5, where a nominal layer for each raster pattern is chosen to form the reference variance. We choose a nominal layer with a variance similar to the mean to reduce sensitivity of the detection method. If the minimum variance is chosen, some nominal layers may result in f-statistics higher than the statistical threshold. Furthermore, the diagonal raster direction exhibits a higher variance than the other two directions, as the raster is composed of varying scan line lengths (refer to Figure 1). Consequently, the signal is not as well represented by an AR model, as some time-varying behavior occurs at the start and end of the layer rasters. This can be resolved with time varying models, which is the subject of future work.

Example layers at $\alpha = 10^{-6}$ (type I error) and window size $M = 300$ are presented in Figure 6 for all raster patterns. The short direction (left) has three example layers. Nominal layer 33 (top) remains entirely below the statistical threshold. The anomalous layer 15 (middle), has a large anomaly at 3 seconds, with an f-statistic nearing 5, corresponding to a variance 5 times the value of the nominal reference. Layer 24 (bottom) also exhibits an anomaly at 1.5 seconds, surpassing the statistical threshold. Notably, the remainder of layer 24 (after 3 seconds) is nominal, falling below the statistical threshold.

Results are similar for the diagonal layers presented in the center of Figure 6. For the nominal layer 34 (top), the moving variance remains below the statistical threshold. In contrast, anomalies surpass the threshold at anomalous locations in layers 16 and 28. Similar results occur for the long direction (right). Nominal layer 35 is close to the threshold, but below it, while anomalous layers 26 and 29 surpass the threshold.

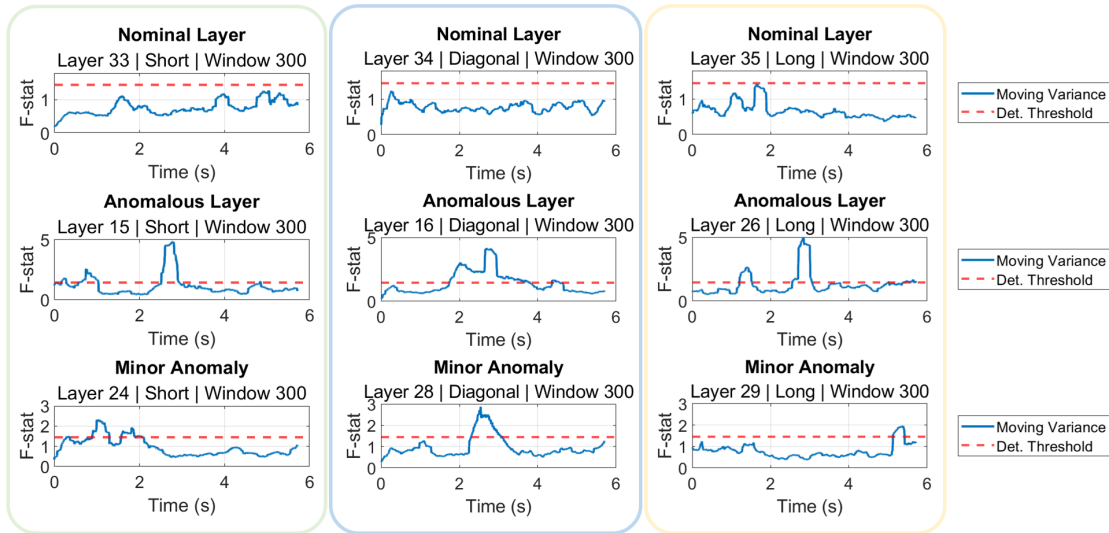


Figure 6. Moving variance for several test layers, short (right, green), diagonal (center, blue), and long (left, yellow) directions with detection threshold $\alpha = 10^{-6}$ (type I error). Nominal layers 33, 34, and 35 (top) experience a low variance in the residuals compared to the anomalous layers 15, 16, and 26 (center). These layers have f-statistics that indicate the peak variance is well above the nominal. Layers 24, 28, and 29 (bottom) have minor anomalies, with the majority of the layer nominal, below the detection threshold.

CONCLUDING REMARKS

This study successfully predicted the melt pool lengths with AR models trained on one nominal layer. These model residuals were used to form a statistical test that correctly determined anomalous behavior for select faults. This research serves as an initial demonstration of this statistical detection method applied to metal AM, although the method is individually trained for each geometry and has difficulty with non-stationary behavior. Future work will focus on a general model that conforms to several input geometries and integrates time-varying behavior. This removes geometric effects from the print, standardizing detection for any geometry.

ACKNOWLEDGMENT

This work was supported in part by the National Science Foundation under CMMI Award #2222250.

REFERENCES

1. Pandiyan, V., G. Masinelli, N. Claire, T. Le-Quang, M. Hamidi-Nasab, C. de Formanoir, R. Esmaeilzadeh, S. Goel, F. Marone, R. Logé, S. Van Petegem, and K. Wasmer. 2022. "Deep learning-based monitoring of laser powder bed fusion process on variable time-scales using heterogeneous sensing and operando X-ray radiography guidance," *Additive Manufacturing*, 58(April), ISSN 22148604, doi:10.1016/j.addma.2022.103007.

2. Jeon, I. and H. Sohn. 2022. "Online melt pool depth estimation in laser metal deposition using a coaxial thermography system," *Journal of Laser Applications*, 34(2):022001, ISSN 1042-346X, doi:10.2351/7.0000618.
3. Rombouts, M., J. Kruth, L. Froyen, and P. Mercelis. 2006. "Fundamentals of Selective Laser Melting of alloyed steel powders," *CIRP Annals*, 55(1):187–192, ISSN 0007-8506, doi:https://doi.org/10.1016/S0007-8506(07)60395-3.
4. Peng, X., L. Kong, W. Han, and S. Wang. 2022. "Multi-Sensor Image Fusion Method for Defect Detection in Powder Bed Fusion," *Sensors (Basel, Switzerland)*, 22(20), ISSN 14248220, doi:10.3390/s22208023.
5. Kudzal, A., B. McWilliams, C. Hofmeister, F. Kellogg, J. Yu, J. Taggart-Scarff, and J. Liang. 2017. "Effect of scan pattern on the microstructure and mechanical properties of Powder Bed Fusion additive manufactured 17-4 stainless steel," *Materials and Design*, 133:205–215, ISSN 18734197, doi:10.1016/j.matdes.2017.07.047.
6. Yeung, H., Z. Yang, and L. Yan. 2020. "A melt pool prediction based scan strategy for powder bed fusion additive manufacturing," *Additive Manufacturing*, 35:101383, ISSN 2214-8604, doi:https://doi.org/10.1016/j.addma.2020.101383.
7. Mahato, V., M. A. Obeidi, D. Brabazon, and P. Cunningham. 2020. "Detecting voids in 3D printing using melt pool time series data," *Journal of Intelligent Manufacturing*, (April), ISSN 15728145, doi:10.1007/s10845-020-01694-8.
8. Chen, A., F. Kopsaftopoulos, and S. Mishra. 2022. "Unsupervised Online Anomaly Detection of Metal Additive Manufacturing Processes via a Statistical Time-Frequency Domain Approach," *ASME International Mechanical Engineering Congress and Exposition*, Volume 1: Acoustics, Vibration, and Phononics, doi:10.1115/IMECE2022-94486.
9. Chen, A., F. Kopsaftopoulos, and S. Mishra. 2023. "An Unsupervised Online Anomaly Detection Method for Metal Additive Manufacturing Processes via a Statistical Time-Frequency Domain Algorithm," *Under review*.
10. Fu, Y., A. R. J. Downey, L. Yuan, T. Zhang, and A. Pratt. 2022. "Machine learning algorithms for defect detection in metal laser-based additive manufacturing : A review," *Journal of Manufacturing Processes*, 75(December 2021):693–710, ISSN 1526-6125, doi:10.1016/j.jmapro.2021.12.061.
11. Fassois, S. D. and J. S. Sakellariou. 2007. "Time-series methods for fault detection and identification in vibrating structures," *Philosophical Transactions of the Royal Society A: Mathematical, Physical and Engineering Sciences*, 365(1851):411–448, doi:10.1098/rsta.2006.1929.
12. Kopsaftopoulos, F. and S. Fassois. 2010. "Vibration based health monitoring for a lightweight truss structure: Experimental assessment of several statistical time series methods," *Mechanical Systems and Signal Processing*, 24:1977–1997, doi:10.1016/j.ymssp.2010.05.013.
13. Ljung, L. 1999. *System Identification: Theory for the User*, Prentice Hall information and system sciences series, Prentice Hall PTR, ISBN 9780136566953.